DESIGN OF PLANAR DUAL AND TRIPLE NARROW-BAND BANDSTOP FILTERS WITH INDEPENDENTLY CONTROLLED STOPBANDS AND IMPROVED SPURIOUS RESPONSE

H. Ning[1, *], J. Wang[1], Q. Xiong[1], and L. Mao[2]

[1]School of Electronic and Information Engineering, Beihang University, Beijing 100191, China

[2]Institute of Intelligent Structure and System, Soochow University, Suzhou, Jiangsu 215006, China

Abstract—A novel design of planar dual and triple narrow-band bandstop filter is presented by adopting the proposed meandered slot defected microstrip structure (MS-DMS) and the simplified spiral microstrip resonator (SSMR). Through this design, the stopbands of the dual- and triple-band bandstop filters can be individually controlled and the improved spurious responses are achieved. First, the fundamental and the first spurious resonances of the MS-DMS and SSMR are analyzed to provide the design rules. Then, by utilizing the prominent stopband of the MS-DMS and the stopband produced by the SSMR coupled to main microstrip line, a dual narrow-band bandstop filter is constructed before its design procedure is outlined. Based on above investigations, a triple narrow-band bandstop filter is implemented by inserting extra SSMRs to another side of the main microstrip line of the dual-band filter to generate a new stopband. To verify the aforementioned design concepts, a dual and triple narrow-band bandstop filter are designed, simulated and tested. Both the simulation and measurement indicate that the fabricated filters exhibit good stopband/passband performance and improved first spurious resonance. Moreover, these filters are simple to design and quite compatible with planar fabrication technique, making them very attractive for practical applications.

1. INTRODUCTION

There is an increasing trend of multifunctional and frequency-agile wireless systems to achieve high integrity, miniaturization, multifunction and flexibility [1–15]. In developing such systems, dual- and triple-band bandstop filters are essential components, which can suppress the unwanted concurrent signals at separate frequencies [7–15]. It has been demonstrated that multi-band bandstop filters have low transmission loss, little group delay, compact size and low cost [7].

There are many effective approaches available to implement filters with dual stopbands response. The dual stopbands close to each other can be obtained by applying frequency-variable transformation to a lowpass prototype in [7]. By employing composite right/left-handed metamaterial transmission lines [8], the dual-band rejection may be realized. Through the use of two-section or tri-section stepped-impedance resonators (SIRs) [9, 10], the layout compactness of dual-band bandstop filter (DBBSF) is achieved. In [11], a compact DBBSF composed of a spur-line structure and a rectangle slot is implemented. However, for the aforementioned filters, it is not convenient to freely control the center frequency of each stopband. A solution to that is to use the open-loop resonators with different lengths [12]. Nevertheless, this filter has a relatively large size and its first spurious resonance is only located at $2f_1$, where f_1 is the center frequency of the first stopband. Therefore, the design of DBBSF with individually controlled stopbands and improved spurious response remains challenging.

The report of triple-band bandstop filter is relatively less, partly due to the design difficulties. A triple-band bandstop filter is presented in [13] by adopting the straight and bent quarter-wavelength resonators to suppress the narrow-band interferences in ultra-wideband (UWB) applications. In [14], the triple-band rejection is obtained through a novel transversal coupling network based on substrate integrated waveguide (SIW) technology. Recently, a compact multi-band bandstop filter composed of a spurline and single rectangular ring resonator is implemented in [15] to block the interfering signals generated by the coexisting wireless access systems. However, the technique that enables the design of a planar triple-band bandstop filter with independent stopbands and high performance needs to be further investigated.

To meet the above requirements, a novel design of dual and triple narrow-band bandstop filters is presented by adopting the meandered slot defected microstrip structure (MS-DMS) and the simplified spiral microstrip resonator (SSMR) in this paper. Firstly, the analysis of the fundamental and the first spurious resonant frequencies of the proposed

MS-DMS and the SSMR are given in detail. Secondly, by using the obvious stopband of the MS-DMS and another stopband generated by the SSMR coupled to the main microstrip line, a dual narrow-band bandstop with separately adjusted stopbands and improved spurious response can be constructed. The design methodology of this filter is described and the design procedure outlined, especially for the stopband design with the MS-DMSs. Then, a triple narrow-band bandstop filter may be realized with extra SSMRs added to another side of the main microstrip line of the dual-band filter. Finally, a dual and triple narrow-band bandstop filter are designed, simulated and measured to validate the proposed design concept.

2. CHARACTERIZATION OF THE RESONATORS

2.1. Meandered Slot Defected Microstrip Structure

Defected microstrip structure (DMS) can be created by etching patterned structure on the signal strip and has been widely used in the applications of microwave devices [16–22], especially for the compact bandstop filter design due to its obvious stopband characteristic and slow-wave effect [19, 20]. Here, the MS-DMS shown in Fig. 1(a) is proposed to achieve compactness and improved first spurious resonance. To this end, the MS-DMS and the recently presented M-shaped DMS in Fig. 1(b) [20] are simulated by the full-wave EM solver Ansoft HFSS with the same occupied area. The substrate employed in the simulations has a relative permittivity of 2.55, a thickness of 1.5 mm, and a loss tangent of 0.002. The simulated transmission responses of both structures are shown in Fig. 2, where we can find that the fundamental resonant frequency of the MS-DMS is at 3.02 GHz lower than that of the M-shaped DMS at 3.78 GHz, and the first spurious resonance of the MS-DMS is located at 9.51 GHz higher than that of the M-shaped DMS at 8.31 GHz. Therefore, the proposed MS-DMS exhibits advantages of a more compact size and improved spurious response compared with the M-shaped DMS.

The underlying physical understanding of the MS-DMS needs to be clarified to provide a design rule. From the perspective of EM wave propagating, the proposed MS-DMS can be regarded as a meandered slotline. When the length of the slotline equals to odd multiple of half guided wavelength λ_g, the transmission zeros are produced. Based on this principle, the fundamental resonant frequency f_1 and the first spurious resonant frequency f_{s1} can be approximately obtained as:

$$f_1 = \frac{c}{2L_{\text{slot}}\sqrt{\varepsilon_1^{\text{slot}}}}, \qquad f_{s1} = \frac{3c}{2L_{\text{slot}}\sqrt{\varepsilon_{s1}^{\text{slot}}}} \qquad (1)$$
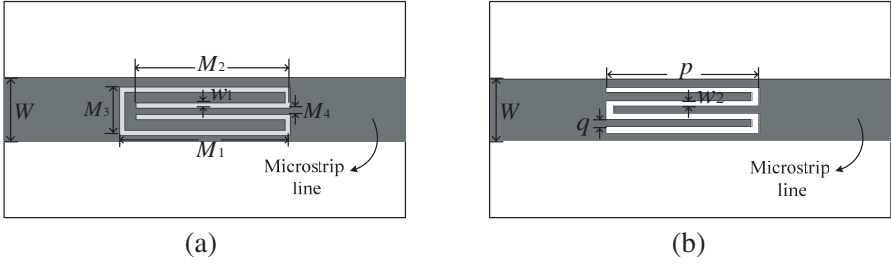
Figure 1. Configuration of (a) the proposed MS-DMS and (b) the M-shaped DMS in [20].
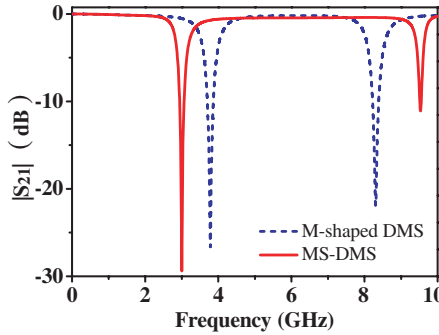

Figure 2. Simulated transmission responses of the MS-DMS and M-shaped DMS with the same occupying area ($W = 4.4\,\text{mm}$, $w_1 = 0.4\,\text{mm}$, $M_1 = 9\,\text{mm}$, $M_2 = 8.0\,\text{mm}$, $M_3 = 3.3\,\text{mm}$, $M_4 = 0.6\,\text{mm}$, $p = 9\,\text{mm}$, $q = 0.57\,\text{mm}$, $w_2 = 0.4\,\text{mm}$).

where c is the free-space speed of light, L_{slot} the total length of the meandered slot. $\varepsilon_1^{\text{slot}}$ and $\varepsilon_{s1}^{\text{slot}}$ are the effective relative permittivity of the slotline at the resonant frequencies, which may be acquired through the closed-form expressions in [23]. For the substrate with a relative dielectric constant of $\varepsilon_r = 2.55$ and a thickness of $h = 1.5\,\text{mm}$ used in our case, the effective relative permittivity of the slotline $\varepsilon_{\text{eff}}^{\text{slot}}$ can be achieved as following:

$$\frac{1}{\sqrt{\varepsilon_{\text{eff}}^{\text{slot}}}} = 1.045 - 0.365 \ln\left(\varepsilon_r\right) + \frac{6.3\left(w/h\right)\varepsilon_r^{0.945}}{\left(238.64 + 100 * w/h\right)}$$

$$- \left[0.148 - \frac{8.81\left(\varepsilon_r + 0.95\right)}{100 * \varepsilon_r}\right] * \ln\left(hf/c\right) \qquad (2)$$

where w is the width of the slotline and f the working frequency.

   The magnetic field distribution of the MS-DMS at the fundamental and the first spurious resonant frequency is shown in Fig. 3, where the magnetic field propagates along the meandered slot at both resonant frequencies. Meanwhile, two maximum occur in Fig. 3(a) and four maximum exist in Fig. 3(b), corresponding to $\lambda_g/2$ and $3\lambda_g/2$ respectively. This demonstrates the validity of our analysis. To further verify that, the effects of the total length of the meandered slot on the resonant frequencies are also analyzed. Fig. 4 shows the variation of the
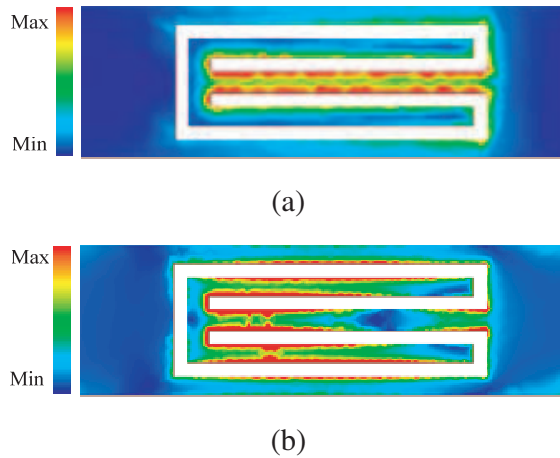
(a)

(b)

Figure 3. Magnetic field distribution of (a) the MS-DMS at the fundamental resonant frequency of 3.02 GHz and (b) the first spurious resonant frequency of 9.51 GHz.
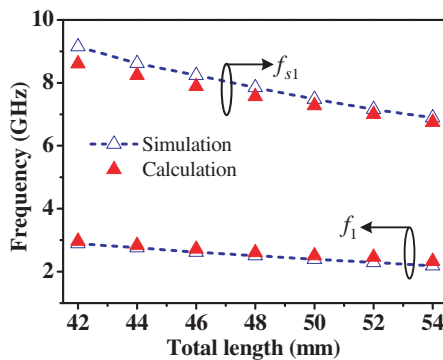
Figure 4. Comparison between the full-wave simulation and theoretical calculation of the fundamental and first spurious resonant frequencies of the MS-DMS.

full-wave simulated and theoretically calculated resonant frequencies as the total length changes. It can be observed that the simulation agrees well with the calculation, especially for the fundamental resonance. The small discrepancy between the simulated and calculated first spurious resonant frequency may be explained from following two perspectives. First, the slotline discontinuities are not considered in our analysis, which are obvious at higher frequencies. Second, the Eq. (2) itself has an average curve fitting error of 0.37% [23].

2.2. Simplified Spiral Microstrip Resonator

It has been shown in [24] that the spiral microstrip resonator has a smaller size compared with the open-loop (half-wavelength) resonator and the improved hairpin resonator; meanwhile, it has an improved first spurious response. The SSMR shown in Fig. 5(a) is used to achieve a suitable narrow bandwidth. Actually, the SSMR can be modeled by a coupled line with two terminals linked by a transmission line and another two terminals open-circuited. The transmission line has the characteristic impedance of Z_t and electrical length of θ_t. The even and odd mode characteristic impedance of the coupled line are Z_e and Z_o, with electrical length θ_e and θ_o correspondingly. Assume that the SSMR is excited at point A, the network model of the SSMR may be derived as depicted in Fig. 5(b). Through this model, we can obtain that:

$$\begin{bmatrix} V_1 \\ I_1 \end{bmatrix} = \begin{bmatrix} A_1 & B_1 \\ C_1 & D_1 \end{bmatrix} \begin{bmatrix} V_2 \\ I_3 \end{bmatrix} \tag{3}$$

$$\begin{bmatrix} V_1 \\ I_2 \end{bmatrix} = \begin{bmatrix} A_2 & B_2 \\ C_2 & D_2 \end{bmatrix} \begin{bmatrix} V_2 \\ -I_3 \end{bmatrix} \tag{4}$$

$$\begin{bmatrix} V_1 \\ I_1 \end{bmatrix} = \begin{bmatrix} A_1 & B_1 \\ C_1 & D_1 \end{bmatrix} \begin{bmatrix} A_2 & -B_2 \\ C_2 & -D_2 \end{bmatrix}^{-1} \begin{bmatrix} V_1 \\ I_2 \end{bmatrix} = \begin{bmatrix} a & b \\ c & d \end{bmatrix} \begin{bmatrix} V_1 \\ I_2 \end{bmatrix} \tag{5}$$

where $a = (-A_1 D_2 - B_1 C_2)/\Delta$, $b = (A_1 B_2 + B_1 A_2)/\Delta$, $c = (-C_1 D_2 - D_1 C_2)/\Delta$, $d = (C_1 B_2 + D_1 A_2)/\Delta$, $\Delta = B_2 C_2 - A_2 D_2$, $A_2 = D_2 = \cos\theta_t$, $B_2 = jZ_t \sin\theta_t$, and $C_2 = j\sin\theta_t/Z_t$. The $ABCD$ parameters of the coupled line with two open-circuited terminals are [25]:

$$A_1 = \frac{Z_e \cot\theta_e + Z_o \cot\theta_o}{Z_e \csc\theta_e - Z_o \csc\theta_o} = D_1 \tag{6}$$

$$B_1 = \frac{j}{2} \frac{Z_e^2 + Z_o^2 - 2Z_e Z_o \left(\cot\theta_e \cot\theta_o + \csc\theta_e \csc\theta_o\right)}{Z_e \csc\theta_e - Z_o \csc\theta_o} \tag{7}$$

$$C_1 = \frac{2j}{Z_e \csc\theta_e - Z_o \csc\theta_o} \tag{8}$$

Then, the input impedance Z_I is expressed as:

$$Z_I = \frac{V_1}{I_I} = \frac{V_1}{I_1 + I_2} = \frac{b}{bc + (1-a)(1+d)} \tag{9}$$

The resonance will happen when $I_1 = -I_2$ (i.e., $Z_I = \infty$). Fig. 6 shows the full-wave simulated and calculated fundamental and first spurious resonant frequencies (denoted by f_2 and f_{s2}), as well as their ratio against the length S_3. It can be clearly seen that the simulations in Fig. 6(a) agree well with the calculations in Fig. 6(b), demonstrating the validity of our analysis. As the length S_3 increases, the fundamental resonant frequency decreases while the variation of the first spurious resonance is very small or even neglected. Therefore, the ratio of the first spurious resonant frequency to the fundamental one is increased. Compared with the conventional half-wavelength resonator with the first spurious resonance at $2f_2$, the improved first spurious resonance can be easily achieved for the SSMR. It is worth pointing out that due to the internal coupling of the SSMR, the fundamental resonance of this resonator will be lower than that of the half-wavelength resonator with the same length, meaning that the SSMR is more compact. For instance, the fundamental resonance of the SSMR is located at 3.24 GHz when the length S_3 is 4.4 mm; while for the half-wavelength resonator with the same length of the SSMR, the fundamental resonant frequency is only 3.84 GHz.
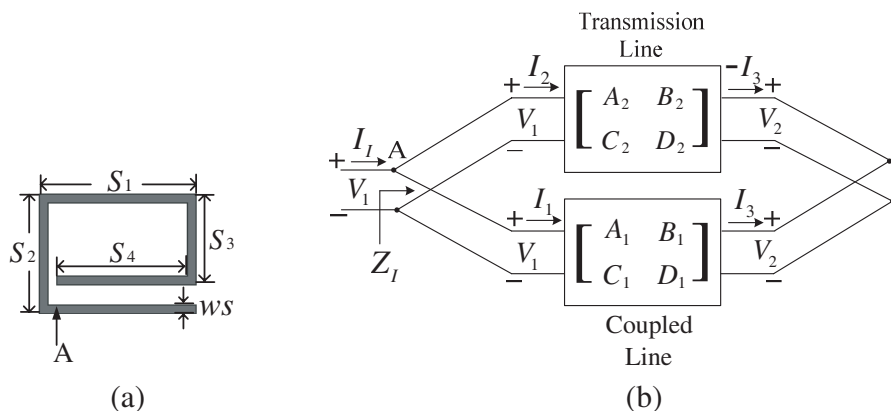

Figure 5. (a) Simplified spiral microstrip resonator. (b) Network model.
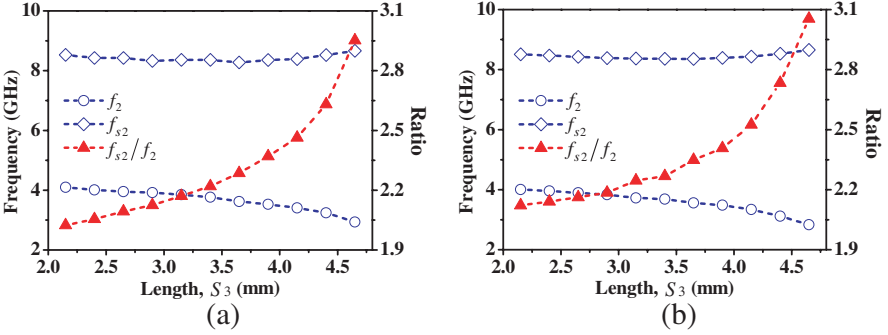
Figure 6. (a) Full-wave simulated and (b) calculated fundamental and first spurious resonant frequencies of SSMR, as well as their ratio against the length S_3 ($S_1 = 7.0$ mm, $S_2 = 5.3$ mm, $S_3 = 4.4$ mm, $S_4 = 6.2$ mm, $ws = 0.4$ mm).

3. DUAL NARROW-BAND BANDSTOP FILTER IMPLEMENTATION

Based on the aforementioned analysis, the MS-DMSs can be used to realize one stopband, and the SSMRs coupled to the main microstrip line may be utilized to implement another stopband. To achieve compactness, the first stopband is determined by the MS-DMS and the second stopband depends on the SSMR. Thus, a dual narrow-band bandstop filter is constructed and its configuration is depicted in Fig. 7. It is noted that these two stopbands can be individually controlled and separately designed since they are generated through different resonators and current paths. Meanwhile, the first spurious resonance f_s of this filter can be approximately estimated as:

$$f_s \approx \min\{f_{s1}, f_{s2}\} \qquad f_{s1} \approx 3f_1, f_{s2} > 2f_2 \qquad (10)$$

As for the stopband design using the SSMRs coupled to the main microstrip line, the conventional design methodology of narrow-band bandstop filter [26] may be applied. The equivalent circuit model for this kind of filter design is illustrated in Fig. 8 and the design flow is outlined as follows. The first step is circuit synthesis, which is based on the operated frequency f_0 and 3-dB fractional bandwidth (FBW). The design parameters are obtained by:

$$\left(\frac{Y_U}{Y_0}\right)^2 = \frac{1}{g_0 g_{n+1}} \qquad (11)$$

$$\left(\frac{b_i}{Y_0}\right) = \left(\frac{Y_U}{Y_0}\right)^2 \frac{g_0}{g_i \Omega_c \text{FBW}} = \frac{f_0}{2\Delta f_{3\,\text{dBi}}} \quad \text{for } i = 1 \text{ to } n \quad (12)$$

$$b_i = 2\pi f_0 C_i = \frac{1}{2\pi f_0 L_i} \quad \text{for} \quad i = 1 \text{ to } n \tag{13}$$

where Y_0 and Y_U denote the terminating admittance and characteristic admittance of immittance inverters; g_i are the element values of lowpass prototype; Ω_c is the normalized cutoff frequency; b_i and $\Delta f_{3\,\text{dBi}}$ are the susceptance slop parameters and 3-dB bandwidths of the serials parallel resonators correspondingly; L_i and C_i are the equivalent inductances and capacitances of each resonator respectively.

The second step is to use the SSMRs with different coupling spaces d_i to the main microstrip line to meet the required susceptance slop parameters. For simplicity, the SSMRs' dimensions are chosen as the same to make them have the same fundamental and first spurious resonant frequency, and the desired coupling space can be obtained with the aid of a full-wave EM solver.

It is worth mentioning that if the radiation loss and conductor loss of the proposed MS-DMS are neglected, its transmission response can be expressed by a parallel LC resonant circuit. Concurrently, the MS-DMS has a high-Q factor. Hence, the above discussed design methodology can be also applied to implement another stopband design using the MS-DMSs if we can obtain proper dimensions of each MS-DMS unit cell to satisfy the required normalized susceptance slop
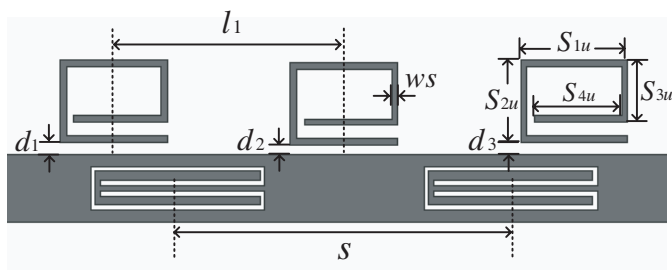

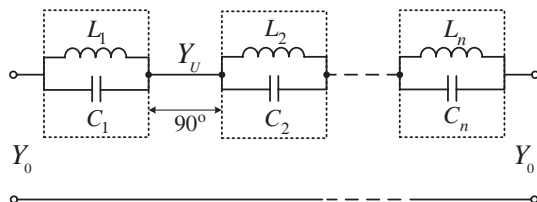**Figure 7.** Configuration of the dual narrow-band bandstop filter.

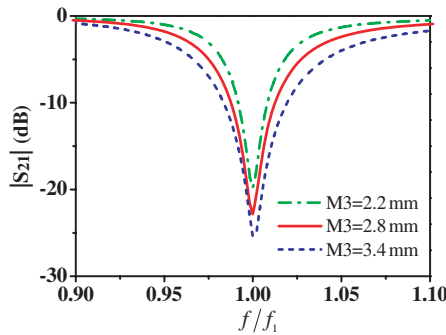**Figure 8.** Equivalent circuit model for the narrow-band bandstop filter design.

Figure 9. Effects of the MS-DMS width M_3 on the stopband bandwidth ($w_1 = 0.3\,\text{mm}$, $M_1 = 9\,\text{mm}$, $M_2 = 8.4\,\text{mm}$, $M_4 = 0.3\,\text{mm}$).

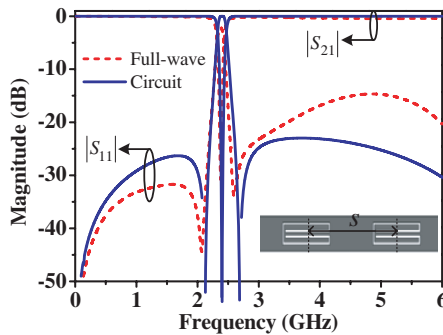**Figure 10.** Circuit and full-wave simulated responses of the designed second-order filter using MS-DMSs ($W = 4.4\,\text{mm}$, $w_1 = 0.25\,\text{mm}$, $M_1 = 11.3\,\text{mm}$, $M_2 = 10.7\,\text{mm}$, $M_3 = 2.0\,\text{mm}$, $M_4 = 0.3\,\text{mm}$, $s = 22.3\,\text{mm}$, $L_1 = L_2 = 5.87\,\text{nH}$, $C_1 = C_2 = 0.75\,\text{pF}$).

parameter of each resonator. Based on the full-wave simulations, it is found that: the stopband bandwidth of the MS-DMS could be adjusted by tuning the width M_3, while the length M_1 and M_2 have little effect on the bandwidth and the resonant frequency mainly depends on that. The simulated transmission responses of the MS-DMS with different widths M_3 are shown in Fig. 9, where the 3-dB FBW of the stopband increases from 5.3% to 11.2% when the width M_3 varies from 2.2 mm to 3.4 mm. Therefore, by finely tuning the dimensions of MS-DMS with the help of a full-wave EM solver, the desired normalized susceptance slop parameter can be achieved. We should remember that the design rule of the MS-DMS discussed in Subsection 2.1 will make this process more efficient.

As an illustrative example of the bandstop filter design using the MS-DMSs, a simple second-order filter with the center frequency of 2.4 GHz and 3-dB FBW of 6.25% is designed following the above procedure. A two-pole Butterworth lowpass prototype is used with the element values $g_0 = g_3 = 1.0$, $g_1 = g_2 = 1.4142$ at $\Omega_c = 1$. Using Eq. (12), we can yield the desired design parameters as:

$$Y_U = Y_0, \quad b_1/Y_0 = b_2/Y_0 = 8.0 \tag{14}$$

Thus, the two MS-DMS unit cells should have the same dimensions. The layout of this designed filter along with its final dimensions is shown in Fig. 10. The full-wave and circuit simulated responses of this filter are also plotted in Fig. 10 and a good agreement is obtained between the two. The small difference in the rejection level of the center frequency of the stopband and the reflection coefficient at higher frequencies results from the radiation loss caused by the MS-DMSs.
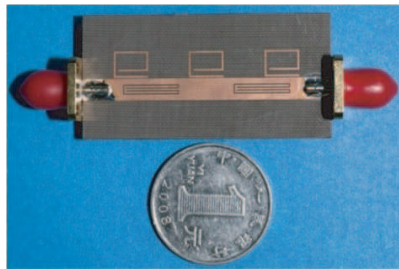

Figure 11. Photograph of the fabricated dual narrow-band bandstop filter. ($S_{1u} = 7.0$ mm, $S_{2u} = 5.3$ mm, $S_{3u} = 4.0$ mm, $S_{4u} = 5.7$ mm, $ws = 0.4$ mm, $d_1 = d_3 = 0.2$ mm, $d_2 = 0.15$ mm, $l_1 = 15.2$ mm, other dimensions are the same with that in Fig. 10).
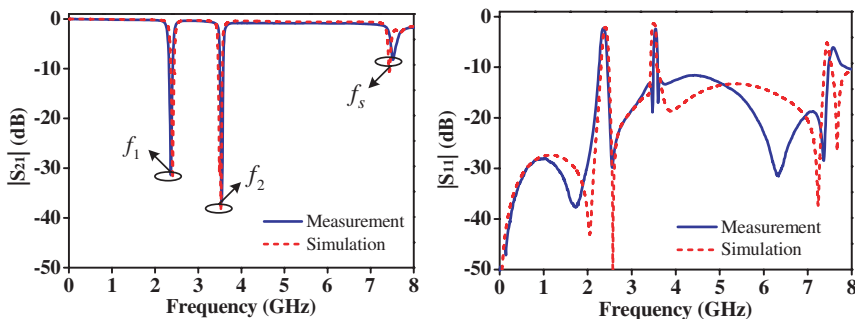

Figure 12. Simulated and measured responses of the fabricated dual narrow-band bandstop filter.

A dual narrow-band bandstop filter is designed according to above design process and simulated by HFSS. The final optimized filter is fabricated on Arlon Cuclad 250 GX(tm) substrate with a relative dielectric constant of 2.55, a thickness of 1.5 mm, and a loss tangent of 0.002. Fig. 11 shows the photograph of the fabricated filter and the simulated and measured responses of this filter are depicted in Fig. 12, showing a good agreement between the two. Some slight discrepancies may be attributed to the fabrication error.

As can be seen in Fig. 12, the measured dual stopbands are centered at 2.37 GHz and 3.54 GHz, with 3-dB FBWs of 6.33% (2.29 GHz–2.44 GHz) and 3.39% (3.48 GHz–3.60 GHz), stopband rejections of 31.4 dB and 36.7 dB respectively. The first spurious resonance is located at 7.52 GHz (i.e., $3.17f_1$). The measured typical insertion loss of the low, middle and upper passband (below 7.52 GHz) is 0.12 dB, 0.40 dB and 0.82 dB correspondingly. The measured return loss is better than 11.5 dB in the whole passbands. It is noticed that due to the utilization of the MS-DMSs, the proposed dual narrow-band bandstop filter is more compact compared with the filter in [12], which also has two independently controlled stopbands. Moreover, unlike the quarter-wavelength resonator filters [13] with the first spurious resonance located at $3f_1$, the improved spurious response of the proposed filter is achieved without needing short-circuit connections to ground through via holes, which makes this filter quite compatible with planar fabrication techniques.

4. TRIPLE NARROW-BAND BANDSTOP FILTER IMPLEMENTATION

Based on above investigations, a third stopband can be generated by simultaneously adding the SSMRs to another side of the main microstrip line of the dual narrow-band bandstop filter. Therefore, a triple narrow-band bandstop filter is constructed and Fig. 13(a) shows its layout. Through this configuration, the triple stopbands can be individually controlled, and the first spurious resonance f_s of this filter may be roughly obtained as:

$$f_s \approx \min\{f_{s1}, f_{s2}, f_{s3}\} \qquad f_{s1} \approx 3f_1, f_{s2} > 2f_2, f_{s3} > 2f_3 \qquad (15)$$

where f_3 is the third fundamental resonant frequency caused by the added SSMR, and f_{s3} is its first spurious resonant frequency.

A triple narrow-band bandstop filter is designed, simulated and measured to verify the proposed design method. The fabricated filter along with its dimensions is shown in Fig. 13(b). The simulated and measured responses of this filter are plotted in Fig. 14 and a

good agreement is obtained. Both the simulation and measurement show that the triple stopbands are located at 2.37 GHz, 3.54 GHz, and 5.01 GHz, with 3-dB FBWs of 6.33% (2.29 GHz–2.44 GHz), 3.95% (3.47 GHz–3.61 GHz) and 3.79% (4.93 GHz–5.12 GHz), stopband rejections of 31.2 dB, 30.9 dB and 40.5 dB correspondingly. The first spurious resonant frequency is 7.52 GHz equal to $3.17f_1$. Thus, the improved spurious response of this filter is obtained. The measured typical insertion losses of the four passbands, which are from lower frequency to higher frequency and below the first spurious resonant frequency, are 0.14 dB, 0.35 dB, 0.50 dB and 0.92 dB respectively. The return loss is better than 10 dB in the whole passbands. It should be noted that the first and second stopband as well as the first spurious resonance of this triple-band filter are almost the same with the aforementioned dual-band filter, further demonstrating our proposed design concept.
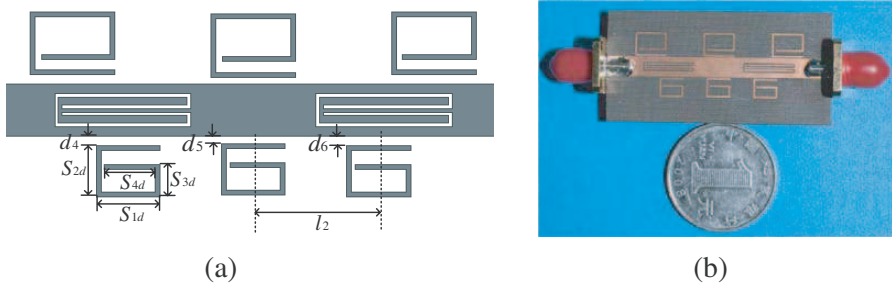

(a)   (b)

Figure 13. (a) Layout of the triple narrow-band bandstop filter. (b) Photograph of the fabricated filter ($S_{1d} = 5.3$ mm, $S_{2d} = 4.3$ mm, $S_{3d} = 2.7$ mm, $S_{4d} = 4.2$ mm, $d_4 = d_6 = 0.24$ mm, $d_5 = 0.2$ mm, $l_2 = 10.4$ mm, other dimensions are the same as that in Fig. 11).
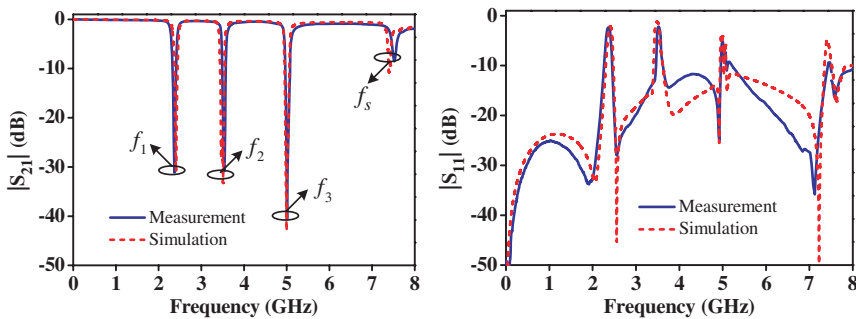

Figure 14. Simulated and measured responses of the fabricated triple narrow-band bandstop filter.

5. CONCLUSION

This paper presents a new design method of planar dual and triple narrow-band bandstop filter. First, the fundamental and the first resonant frequencies of the proposed MS-DMS are analyzed from the perspective of EM wave propagation, and the resonances of the SSMR are discussed based on its network model. Second, by making use of the characteristics of the MS-DMS and the SSMR coupled to the main microstrip line, a dual and triple narrow-band bandstop filter are implemented, which have independently controlled stopbands and improved first spurious resonance. Both the simulation and measurement of the fabricated filters validate our proposed design concept, and show good passband performance and stopband rejection. Easy to design and fabricate, the developed filters can be a good candidate for the application of multi-band wireless communication systems.

ACKNOWLEDGMENT

REFERENCES

1. Yang, R.-Y., K. Hon, C.-Y. Hung, and C.-S. Ye, "Design of dual-band bandpass filters using a dual feeding structure and embedded uniform impedance resonators," *Progress In Electromagnetic Research*, Vol. 105, 93–102, 2010.

2. Ma, D.-C., Z.-Y. Xiao, L.-L. Xiang, X.-H. Wu, C.-Y. Huang, and X. Kou, "Compact dual-band bandpass filter using folded SIR with two stubs for WLAN," *Progress In Electromagnetic Research*, Vol. 117, 357–364, 2011.

3. Chaudhary, G., Y. Jeong, K. Kim, and D. Ahn, "Design of dual-band bandpass filters with controllable bandwidths using new mapping function," *Progress In Electromagnetic Research*, Vol. 124, 17–34, 2012.

4. Chiou, Y.-C. and J.-Y. Kuo, "Planar multiband bandpass filter with multimode stepped-impedance resonators," *Progress In Electromagnetic Research*, Vol. 114, 129–144, 2011.

5. Chen, J., J.-Z. Chen, B. Wu, Y. L. Zhang, and C.-H. Liang, "Design of triple-band microstrip filter with transmission zeros

using open stubs," *Journal of Electromagnetic Waves and Application*, Vol. 26, No. 4, 525–534, 2012.

6. Chen, W.-Y., M.-H. Weng, S.-J. Chang, H. Kuan, and Y.-H. Su, "A new tri-band bandpass filter for GSM, WiMAX, and ultra-wideband responses by using asymmetric stepped impedance resonators," *Progress In Electromagnetic Research*, Vol. 124, 365–381, 2012.

7. Uchida, H., H. Kamino, K. Totani, N. Yoneda, M. Miyazaki, Y. Konishi, S. Makino, J. Hirokawa, and M. Ando, "Dual-band-rejection filter for distortion reduction in RF transmitters," *IEEE Trans. Microwave Theory Tech.*, Vol. 52, No. 11, 2550–2556, 2004.

8. Tseng, C.-H. and T. Itoh, "Dual-band bandpass and bandstop filters using composite right/left-handed metamaterial transmission lines," *IEEE MTT-S Int. Microwave Symp. Dig.*, 931–934, 2006.

9. Chin, K.-S., J. H. Yeh, and S. H. Chao, "Compact dual-band bandstop filters using stepped-impedance resonators," *IEEE Microwave Wireless Comp. Lett.*, Vol. 17, No. 12, 849–851, 2007.

10. Chin, K.-S. and C.-K. Lung, "Miniaturized microstrip dual-band bandstop filters using tri-section stepped-impedance resonators," *Progress In Electromagnetic Research C*, Vol. 10, 37–48, 2009

11. Cheng, D., H.-C. Yin, and H.-X. Zheng, "A compact dual-band bandstop filter with defected microstrip slot," *Journal of Electromagnetic Waves and Application*, Vol. 26, No. 10, 1374–1380, 2012.

12. Vegesna, S. and M. Saed, "Microstrip dual-band bandpass and bandstop filters," *Microwave Opt. Technol. Lett.*, Vol. 54, No. 1, 168–171, 2012.

13. Rambabu, K., M. Y.-W. Chia, K. Chan, and J. Bornemann, "Design of multiple-stopband filters for interference suppression in UWB applications," *IEEE Trans. Microwave Theory Tech.*, Vol. 58, No. 8, 3333–3338, 2006.

14. Han, S. H., X. L. Wang, and Y. Fan, "Analysis and design of multiple-band bandstop filters," *Progress In Electromagnetic Research*, Vol. 70, 297–306, 2007.

15. Wang, Y., J. Zhou, and W. Hong, "A multiband bandstop filters using a single ring resonator for a wireless access communication system," *Microwave Journal*, Vol. 54, No. 3, 102–108, 2011.

16. Kazerooni, M. and A. Cheldavi, "Simulation, analysis, design and applications of array defected microstrip structure (ADMS) filters using rigorously coupled multi-strip (RCMS) method," *Progress In Electromagnetic Research*, Vol. 63, 193–207, 2006.

17. Fallahzadeh, S. and M. Tayarani, "A new microstrip UWB bandpass filter using defected microstrip structures," *Journal of Electromagnetic Waves and Application*, Vol. 24, No. 7, 893–902, 2010.

18. Barbarino, S. and F. Consoli, "UWB circular slot antenna provided with an inverted-L notch filter for the 5 GHz WLAN band," *Progress In Electromagnetic Research*, Vol. 104, 1–13, 2010.

19. Xiang, Q.-Y., Q.-Y. Feng, and X.-G. Huang, "Bandstop filter based on complementary split ring resonators defected microstrip structure," *Journal of Electromagnetic Waves and Application*, Vol. 25, No. 13, 1895–1908, 2011.

20. La, D., Y. Lu, S. Sun, N. Liu, and J. Zhang, "A novel compact bandstop filter using defected microstrip structure," *Microwave Opt. Technol. Lett.*, Vol. 53, No. 2, 433–435, 2011.

21. Kazerooni, M. and M. Aghalari, "Size reduction and harmonic suppression of rat-race hybrid coupler using defected microstrip structure," *Progress In Electromagnetic Research Letters*, Vol. 26, 87–96, 2011.

22. Cheng, D., H.-C. Yin, and H.-X. Zheng, "Investigation on a defected microstrip structure and applications in designing microstrip filters," *Journal of Electromagnetic Waves and Application*, Vol. 26, No. 10, 1332–1340, 2012.

23. Gupta, K. C., R. Garg, I. Bahl, and P. Bhartia, *Microstrip Lines and Slotlines*, 2nd Edition, Artech House, Norwood, MA, 1996.

24. Joubert, J., "Spiral microstrip resonators for narrow-stopband filters," *IEE Proc.-Microwave Antennas Propag.*, Vol. 150, No. 6, 493–496, 2003.

25. Zysman, G. I. and A. Johnson, "Coupled transmission line networks in an inhomogeneous dielectric medium," *IEEE Trans. Microwave Theory Tech.*, Vol. 17, No. 10, 753–759, 1969.

26. Hong, J. S. and M. J. Lancaster, *Microstrip Filters for RF/Microwave Applications*, John Wiley & Sons, New York, 2001.